Chemistry Europe
European Chemical Societies Publishing

WILEY VCH

# Excellence in Chemistry Research


## Announcing our new flagship journal

- Gold Open Access
- Publishing charges waived
- Preprints welcome
- Edited by active scientists

## Meet the Editors of *ChemistryEurope*

**Luisa De Cola**
Università degli Studi di Milano Statale, Italy

**Ive Hermans**
University of Wisconsin-Madison, USA

**Ken Tanaka**
Tokyo Institute of Technology, Japan

ChemCatChem

Research Article
doi.org/10.1002/cctc.202201354

Chemistry Europe
European Chemical Societies Publishing

www.chemcatchem.org

# $MO_x$@$VO_x$-Pd-type Nanorods and Nanotubes as Catalysts for Selective Reduction of NO

Lucas Warmuth,[a] Patrick Lott,[b] Olaf Deutschmann,*[b] and Claus Feldmann*[a]

Vanadium oxide ($VO_x$-Pd) nanotubes as well as $VO_x$-coated ZnO nanorods (ZnO@$VO_x$-Pd) and $VO_x$-coated, layered-titania nanotubes (l-$TiO_2$@$VO_x$-Pd) are decorated with Pd nanoparticles and evaluated for selective catalytic reduction with hydrogen ($H_2$-SCR) for the first time. The nanostructures exhibit lengths of 300 to 700 nm, diameters of 20–100 nm and, in the case of the nanotubes, an inner tube diameter of about 10 nm. Pd nanoparticles (14±5 nm) are well-dispersed over the respective nanorod/nanotube nanostructure. Structure and composition are characterized by SEM, TEM, EDXS with element mapping, XPS, FT-IR, XRD, and sorption analysis. Thermal analysis indicates the nanostructures to be thermally stabile up to 350 °C ($VO_x$), and 500 °C (ZnO@$VO_x$, l-$TiO_2$@$VO_x$). All catalysts are tested for their activity in regard of the selective catalytic reduction of NO with $H_2$, revealing a significant impact of the catalyst support on both activity and selectivity. Specifically, l-$TiO_2$@$VO_x$ nanotubes show promising properties with an activity up to 70 % and a selectivity up to 80 % $N_2$.

## Introduction

Vanadium oxides ($VO_x$) are widely used for redox catalysis and specifically characterized by facile switching between the oxidation states $V^{+IV}$ and $V^{+V}$ as well as by fast oxygen release and incorporation.[1] Most often $VO_x$-based catalysts are used in the context of sensing,[1d] photocatalysis,[2] or electrocatalysis.[3] $VO_x$ is also known as an integral component of selective catalytic reduction (SCR) catalysts that allow for a reduction of $NO_x$ emissions with $NH_3$ in the exhaust stream of lean-operated diesel or natural gas engines.[4] In the combination with palladium (Pd), $VO_x$ turned out to be promising for selective catalytic reduction of $NO_x$ emissions of hydrogen-fueled combustion engines in the so-called $H_2$-SCR process according to the equation: $2\ NO + 2\ H_2 \rightarrow N_2 + 2\ H_2O$.[5] Herein, $VO_x$ usually serves as reducible support material that promotes the formation of $NH_x$ species, namely $NH_3$ and $NH_4^+$, which have been reported to be essential intermediates in the selective catalytic reduction of NO with $H_2$.[6] Palladium, which serves as oxidation catalyst in lean exhausts, i.e. for hydrocarbon or NO oxidation, and which is also used in three-way catalysts (TWC) for cleaning stoichiometric exhaust gases,[7] has a twofold role. On the one hand, Pd adsorbs and activates $H_2$ from the gas phase,[5a] and on the other hand, it catalyzes the reaction between NO and $NH_x$ species to ultimately form $N_2$ and $H_2O$.[6] Both requires a close contact between the noble metal and the metal-oxide support material, since the spillover of surface species between the noble metal and the support material has been identified to be a key for high NO conversion.[8] Beside the intended nitrogen, the reaction also often yields certain amounts of toxic $NH_3$ and the greenhouse-gas $N_2O$ as by-products.[9] Increasing activity and selectivity of the $H_2$-SCR process and suppressing $NH_3$ and $N_2O$ as undesired by-products require additional research efforts, improved understanding, and optimized catalyst materials.

Motivated by previous studies that point to the suitability of $VO_x$-Pd for selective catalytic reduction of $NO_x$ by $H_2$,[5,6] we here aim at investigating nanorod- and nanotube-like $VO_x$-Pd catalysts for $H_2$-SCR. For such catalyst shapes, generally, a high active surface and a high thermal stability can be expected.[10] Pd-impregnated $VO_x$ nanotubes, to the best of our knowledge, have been rarely applied for redox catalysis and were yet only described for the electrooxidation of methanol.[11] Moreover, promising results have been reported for $NH_3$-SCR over $VO_x$/$WO_x$-modified or -decorated titania nanotubes.[12] Here, we report on the synthesis of $VO_x$-Pd nanotubes, ZnO@$VO_x$-Pd nanorods, and l-$TiO_2$@$VO_x$-Pd nanotubes (l-$TiO_2$: layered titania) and their evaluation in regard of the catalytic reduction of $NO_x$ with $H_2$ as a novel catalyst formulation for emission control of modern hydrogen-combustion engines.

## Results and Discussion

### Characterization of $VO_x$ nanotubes

Following a procedure reported by Spahr *et al.*,[13] $VO_x$ nanotubes were prepared by autoclaving $V_2O_5$ in an ethanol-water

[a] Dr. L. Warmuth, Prof. C. Feldmann
Institute of Inorganic Chemistry (IAC)
Karlsruhe Institute of Technology (KIT)
Engesserstraße 15
D-76131 Karlsruhe (Germany)
E-mail: claus.feldmann@kit.edu

[b] Dr. P. Lott, Prof. O. Deutschmann
Institute for Chemical Technology and Polymer Chemistry (ITCP)
Karlsruhe Institute of Technology (KIT)
Engesserstraße 20
76131 Karlsruhe (Germany)
E-mail: deutschmann@kit.edu

Supporting information for this article is available on the WWW under https://doi.org/10.1002/cctc.202201354

© 2022 The Authors. ChemCatChem published by Wiley-VCH GmbH. This is an open access article under the terms of the Creative Commons Attribution Non-Commercial NoDerivs License, which permits use and distribution in any medium, provided the original work is properly cited, the use is non-commercial and no modifications or adaptations are made.


© 2022 The Authors. ChemCatChem published by Wiley-VCH GmbH

18673899, 0, Downloaded from https://chemistry-europe.onlinelibrary.wiley.com/doi/10.1002/cctc.202201354 by Karlsruher Inst F. Technologie, Wiley Online Library on [03/02/2023]. See the Terms and Conditions (https://onlinelibrary.wiley.com/terms-and-conditions) on Wiley Online Library for rules of use; OA articles are governed by the applicable Creative Commons License

mixture in the presence of dodecylamine at 180 °C for 7 days. Accordingly, $VO_x$ nanotubes were either prepared in the liquid phase with vanadium(V) alkoxides, $VOCl_3$, or $V_2O_5$ as the starting materials.[13,14] Herein, the oxidation state of vanadium was deduced via magnetic measurements to +4.8. For all these approaches, long-chained high-molecular weight stabilizers such as dodecylamine are required for exfoliation and surface stabilization of the $VO_x$ nanotubes.[14a] Subsequent to the synthesis, the structure and shape of the as-prepared dark green solid was examined by X-ray diffraction (XRD) and high-annular dark field (HAADF) scanning transmission electron microscopy (STEM). XRD shows reflexes at low two-theta values, which were calculated to 2.75 nm (Figure 1a), and thus, point to a material with large lattice spacing. HAADF-STEM overview images show multi-walled nanotubes with uniform shape, a length of 700 ± 300 nm and a diameter of 100 ± 25 nm (Figure 1b). High-resolution images confirm the tube-like structure with a wall thickness of 40–50 nm and an inner tube of about 10 nm in diameter (Figure 1c). The mean oxidation state of vanadium was determined by X-ray photoelectron spectroscopy (XPS) to 4.78 (Figure 1d). Together with elemental analysis (EA; *SI: Table S1*), a mean sum formula of $VO_{2.39}(C_{12}H_{28}N)_{0.21}$ can be deduced, which compares to literature data of comparable $VO_x$ nanotubes.[13,14a,15] Fourier-transform infrared (FT-IR) spectroscopy, finally, shows the presence of dodecylamine, which is adhered on the nanotube surface (Figure S1).

Ultimately, the as-prepared $VO_x$ nanotubes were impregnated with Pd nanoparticles. To this concern, a solution of $PdAc_2$ in acetone was dropped on the $VO_x$ nanotube powder. Due to the low surface tension of the solution, palladium was homogenously distributed by capillary forces. Thereafter, acetone was removed by evacuation and $Pd^{2+}$ reduced by purging with $H_2$:$N_2$ (10:90) at room temperature.[16] The presence of Pd nanoparticles, their size and distribution over the $VO_x$ nanotubes were examined by EDXS and TEM (Figure 2), uncovering a homogeneous Pd distribution with 2.0 wt-% loading and a mean size of 14 ± 5 nm. The size of the Pd nanoparticles could hardly be reduced further due to redox interaction with the support. Thus, the $VO_2^+/VO^{2+}$ redox couple ($E_0(VO_2^+/VO^{2+}) = 1.0$ V) has a similar redox potential as the $Pd^{2+}/Pd$ redox couple ($E_0(Pd^{2+}/Pd^0) = 1.0$ V),[16] so that a reductive treatment with $H_2$:$N_2$ promotes the reduction of both. This prevents a distinct seed formation of Pd particles and enhances seed growth by continuous $VO_2^+/VO^{2+}$-driven reduction and reoxidation.

## ZnO@$VO_x$ nanorods and l-$TiO_2$@$VO_x$ nanotubes

Since the catalytic activity typically not only depends on the metal catalyst but also on the respective support material, we have modified the $VO_x$ support by ZnO as a basic oxide and $TiO_2$ as an acidic oxide to probe the effect on NO reduction by selective catalytic reduction with $H_2$. To this concern, ZnO@$VO_x$-Pd nanorods were prepared with ZnO nanorods realized following a literature recipe.[17] As a basic metal oxide ZnO exhibits a positively charged surface at neutral pH.[18] Upon addition of a solution of $VO(SO_4)$, the as-formed $[(VO)_2(OH)_5]^-$ ions[16] are adhered on the ZnO nanorods, which promotes the formation of a ZnO@$VO_x$ core@shell structure (Figure 3a–c) that exhibits an overall vanadium content of 5 wt-%. HAADF-STEM overview images show the nanorods with a length of 700 ± 300 nm and a diameter of 40 ± 10 nm (Figure 3a,d). High-resolution images confirm the length and diameter of the nanorods (Figure 3b). EDXS element mappings confirm the core@shell structure of the nanorods with a uniform coverage of the ZnO nanorods with $VO_x$ (Figure 3c,e,f), whereas X-ray diffraction indicates the amorphicity of the mentioned layer (*SI: Figure S2*). Finally, the ZnO@$VO_x$ nanorods were impregnated with Pd nanoparticles, following the procedure described for the $VO_x$ nanotubes to result in ZnO@$VO_x$-Pd nanorods with a Pd loading of 2.1 wt-% (Figure 3g).

In addition to the ZnO@$VO_x$-Pd nanorods, l-$TiO_2$@$VO_x$-Pd nanotubes were prepared. These l-$TiO_2$ nanotubes were obtained via a two-step process similar to our previously reported approach.[19] First of all, titanium metal was oxidized

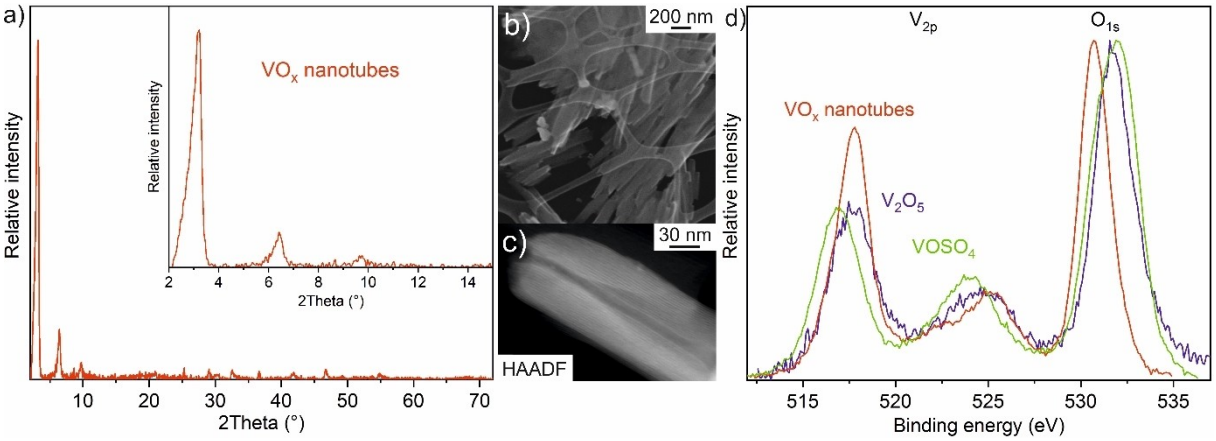


**Figure 1.** Characterization of $VO_x$ nanotubes: (a) XRD with low 2-theta area as inset, (b) HAADF-STEM overview image, (c) HAADF-STEM detail image of a single nanotube, (d) XPS to indicate the oxidation state of vanadium showing the $V_{2p}$ and $O_{1s}$ region with $V_2O_5$ (blue) and $VO(SO_4)$ (green) as references.


© 2022 The Authors. ChemCatChem published by Wiley-VCH GmbH

18673899, 0, Downloaded from https://chemistry-europe.onlinelibrary.wiley.com/doi/10.1002/cctc.202201354 by Karlsruher Inst. F. Technologie, Wiley Online Library on [03/02/2023]. See the Terms and Conditions (https://onlinelibrary.wiley.com/terms-and-conditions) on Wiley Online Library for rules of use; OA articles are governed by the applicable Creative Commons License

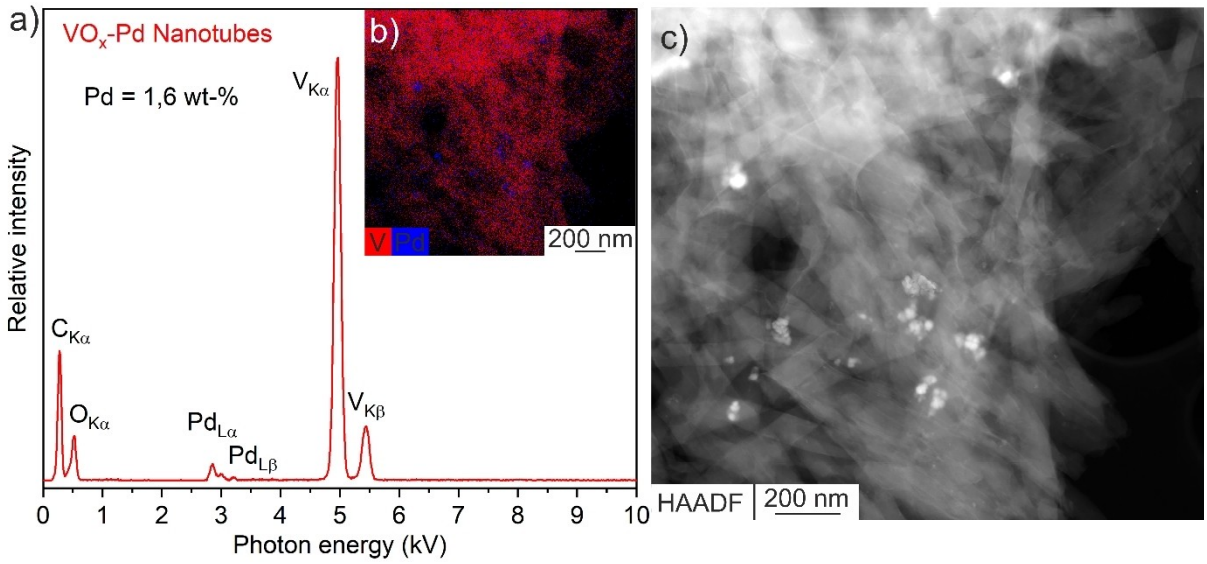


**Figure 2.** $VO_x$ nanotubes after impregnation with Pd nanoparticles: (a) EDXS, (b) EDXS element mapping, and (c) HAADF-STEM image.

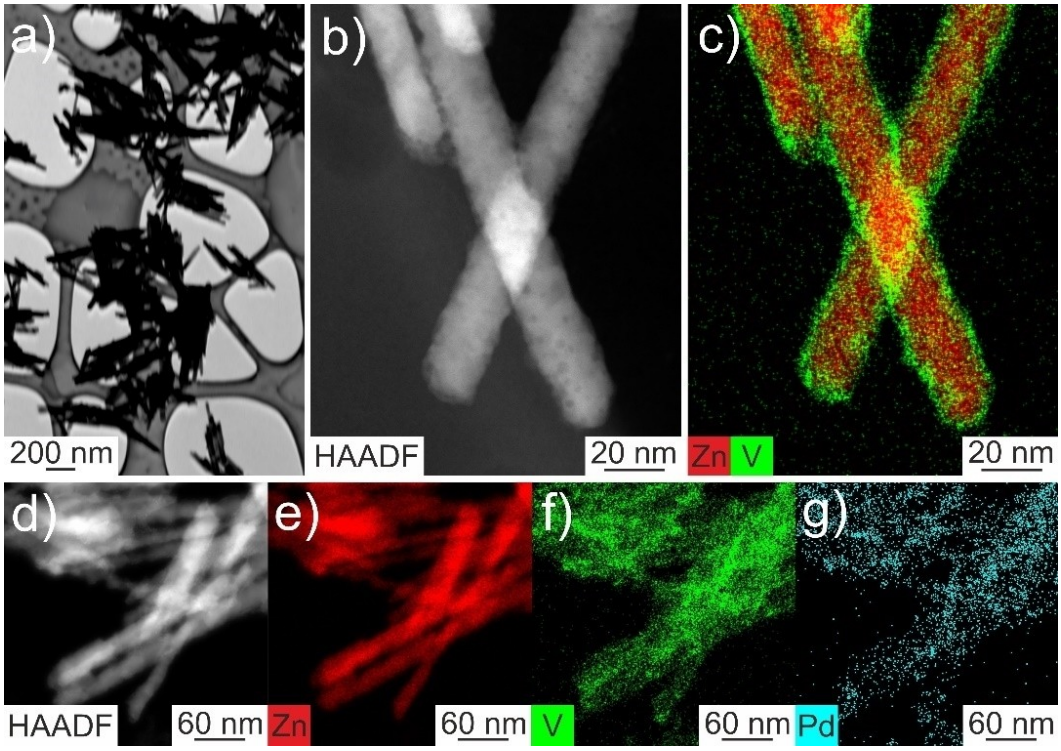


**Figure 3.** ZnO@$VO_x$ nanorods: (a) HAADF-STEM overview image, (b,d) HAADF-STEM detail image, (c,e,f,g) EDXS element mapping prior (c) and after Pd nanoparticle impregnation (e-g).

under strongly alkaline conditions in aqueous NaOH to obtain $Na_2Ti_3O_7$ as a layer-type sodium titanate. These titanate layers of this intermediate compound were then exfoliated under acidic conditions with exchange of $Na^+$ cations by $H^+$, followed by a self-rolling process of the protonated titania layers to form layered-$TiO_2$ (l-$TiO_2$) nanotubes. The as-prepared l-$TiO_2$ nanotubes were then coated by $VO_x$, in principle, similarly to the aforementioned ZnO nanorods by addition of a solution of $VO(SO_4)$. In contrast to ZnO, however, l-$TiO_2$ nanotubes are negatively charged in this pH range (pH = 6; *SI: Figure S3*),[20] so that the diffusion of $[(VO)_2(OH)_5]^-$ ions to the nanotube surface is slow. Consequently, only a limited $VO_x$ content was deposited on the l-$TiO_2$ nanotubes ($\leq$ 1 wt-% V). A neutralization of the l-$TiO_2$ nanotube suspension should allow to tackle this limitation


© 2022 The Authors. ChemCatChem published by Wiley-VCH GmbH

18673899, 0, Downloaded from https://chemistry-europe.onlinelibrary.wiley.com/doi/10.1002/cctc.202201354 by Karlsruher Inst F. Technologie, Wiley Online Library on [03/02/2023]. See the Terms and Conditions (https://onlinelibrary.wiley.com/terms-and-conditions) on Wiley Online Library for rules of use; OA articles are governed by the applicable Creative Commons License

in order to reach a higher $VO_x$ loading.[16] Indeed, the addition of simple aqueous NaOH or KOH results in a higher $VO_x$ loading (*SI: Figure S4*). Alkali metal cations, however, are also known as catalyst poisons.[16] Hence, to obtain alkali-metal-free catalysts, diluted aqueous ammonia turned out to be more sufficient as a base and – similar to NaOH or KOH – results in a homogeneous $VO_x$ coating of the l-$TiO_2$ nanotubes with vanadium contents of 5–6 wt-% (Figure 4a–c). STEM overview images prove the presence of nanotubes with a length of 300 ± 50 nm, a diameter of 15 ± 5 nm, and an inner tube diameter of 7 ± 1 nm (Figure 4a,d). High-resolution images confirm length and diameter of the nanorods (Figure 4d). EDXS element mappings prove the core@shell structure of the nanotubes with a uniform coverage of the l-$TiO_2$ nanotubes with $VO_x$ (Figure 4b,c,e,f), whereas the crystallinity of the nanotubes remained unaffected (*SI: Figure S5*). Finally, the l-$TiO_2$@$VO_x$ nanotubes were also impregnated with Pd nanoparticles, following the procedure described for the $VO_x$ nanotubes to result in l-$TiO_2$@$VO_x$-Pd nanotubes with 2.6 wt-% Pd (Figure 4g).

### Thermal stability of $MO_x$@$VO_x$-based supports

For catalytic applications, the thermal stability of the support is an important feature. To this concern, thermogravimetry (TG) and STEM measurements were performed, starting with the $VO_x$ nanotubes. TG shows evaporation of surface-adhered dodecylamine at temperatures >180 °C (Figure 5a), which does not affect the morphological stability of the $VO_x$ nanotubes. According to STEM images, they retain their nanotubular morphology up to a temperature of 350 °C (Figure 5e). Beyond this temperature, the nanotubes decompose with formation of spherical nanoparticles, 50–100 nm in size, which are embedded in a carbon matrix (Figure 5f). The total mass loss of the $VO_x$ nanotubes at 1,000 °C is 33.9 %, which is close to the amount of dodecylamine deduced from EA data (30.2 %; *SI: Table S1*). This remaining small difference between TG and EA data (3.3 %) can be ascribed to the different combustion temperatures (TG: 1,000 °C, EA: 1,150 °C), and water adsorbed on the surface of the $VO_x$ nanotubes. The latter was confirmed by Fourier-transform infrared (FT-IR) spectroscopy of the as-prepared $VO_x$ nanotubes showing vibrations at 3600–3000 $cm^{-1}$ ($\nu$(O–H)) and 1650 $cm^{-1}$ ($\delta(H_2O)$) (*SI: Figure S1*).

Subsequent to the $VO_x$ nanotubes, the thermal stability of the ZnO@$VO_x$ nanorods and l-$TiO_2$@$VO_x$ nanotubes was evaluated (Figure 5). For both, the thermal decomposition starts with the loss of surface-adsorbed water and hydroxyl-associated species below 200 °C with a mass loss of only 3.2 % for ZnO@$VO_x$ and 17 % for l-$TiO_2$@$VO_x$ (Figure 5a). This comparably high value for l-$TiO_2$@$VO_x$ relates to the significantly higher surface area of these nanotubes (l-$TiO_2$@$VO_x$ nanotubes: 387 $m^2/g$ *versus* ZnO@$VO_x$ nanorods: 27 $m^2/g$ and $VO_x$ nanotubes: 25 $m^2/g$). A slight mass increase at high temperatures (> 600 °C) is observed for all samples and can be ascribed to $VO_x$ oxidation. According to STEM images, shape and structure of the ZnO@$VO_x$ nanorods and l-$TiO_2$@$VO_x$ nanotubes was retained

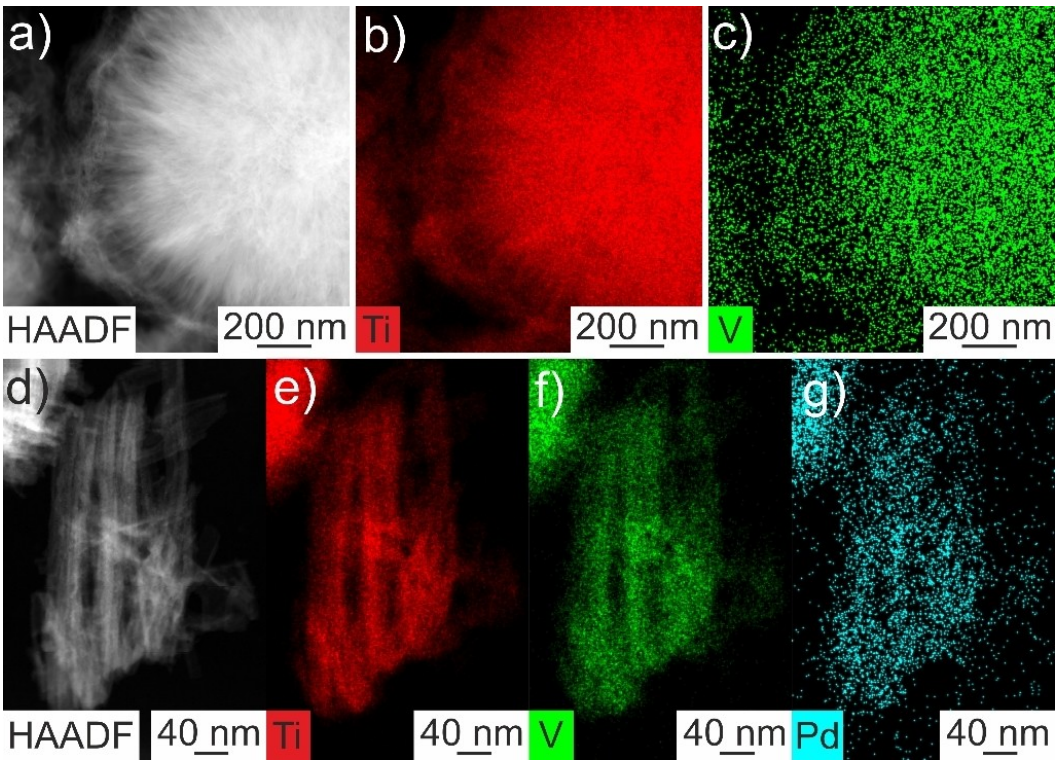


**Figure 4.** L-$TiO_2$@$VO_x$ nanotubes: (a) HAADF-STEM overview image, (b,d) HAADF-STEM detail image, (c,e,f,g) EDXS element mapping prior (b,c) and after Pd nanoparticle impregnation (e-g).


© 2022 The Authors. ChemCatChem published by Wiley-VCH GmbH

18673899, 0, Downloaded from https://chemistry-europe.onlinelibrary.wiley.com/doi/10.1002/cctc.202201354 by Karlsruher Inst. F. Technologie, Wiley Online Library on [03/02/2023]. See the Terms and Conditions (https://onlinelibrary.wiley.com/terms-and-conditions) on Wiley Online Library for rules of use; OA articles are governed by the applicable Creative Commons License

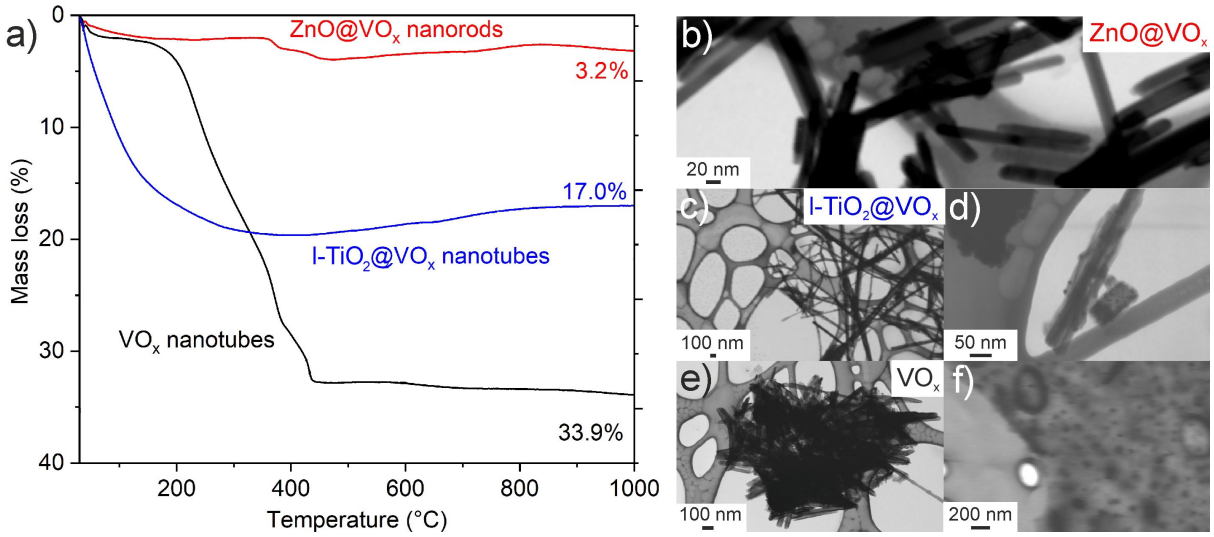


**Figure 5.** Thermal stability of $VO_x$ nanotubes, ZnO@$VO_x$ nanorods, and l-$TiO_2$@$VO_x$ nanotubes: a) TG analysis in an $O_2/N_2$ (20:80) atmosphere; b,c,e) TEM images of the nanostructures after heating to 400 °C ($VO_x$ nanotubes: 350 °C); d,f) TEM images of the nanostructures after heating to 500 °C.

after heating to 400 (Figure 5b,c,e) and 500 °C, respectively (Figure 5d,f). For the ZnO@$VO_x$ nanorods, thermal sintering of the nanorods even occured above 600 °C, which is due to the well-known Hüttig temperature ($T_{Hüttig}$ = 674 °C).[21] In sum, the deposition of $VO_x$ on ZnO nanorods and l-$TiO_2$ nanotubes as supports results in an increased thermal stability in comparison to the $VO_x$ nanotubes.

## Catalytic activity

The catalytic properties of the $VO_x$-Pd nanotubes, ZnO@$VO_x$-Pd nanorods, and l-$TiO_2$@$VO_x$-Pd nanotubes were evaluated in regard of the catalytic reduction of $NO_x$ with $H_2$ ($H_2$-SCR process).[9a] Thus, the catalytic activity was examined in a catalyst testing bench by exposing the respective sample to a gas atmosphere containing 0.1 vol.-% NO, 0.5 vol.-% $H_2$, and 10 vol.-% $O_2$ in nitrogen as inert carrier gas with temperatures of 100 °C to 300 °C, using a space velocity of approximately 80,000 $h^{-1}$. The resulting gas concentrations throughout the entire heating and cooling cycle for the $VO_x$-Pd nanotubes, ZnO@$VO_x$-Pd nanorods, and l-$TiO_2$@$VO_x$-Pd nanotubes are displayed in Figures 6–8 (*SI: Figures S6–S9*).

For the $VO_x$-Pd nanotubes, a considerable NO conversion started at 200 °C and culminates in a maximum conversion of 27 % at 283 °C (Figure 6). Further heating is accompanied with a

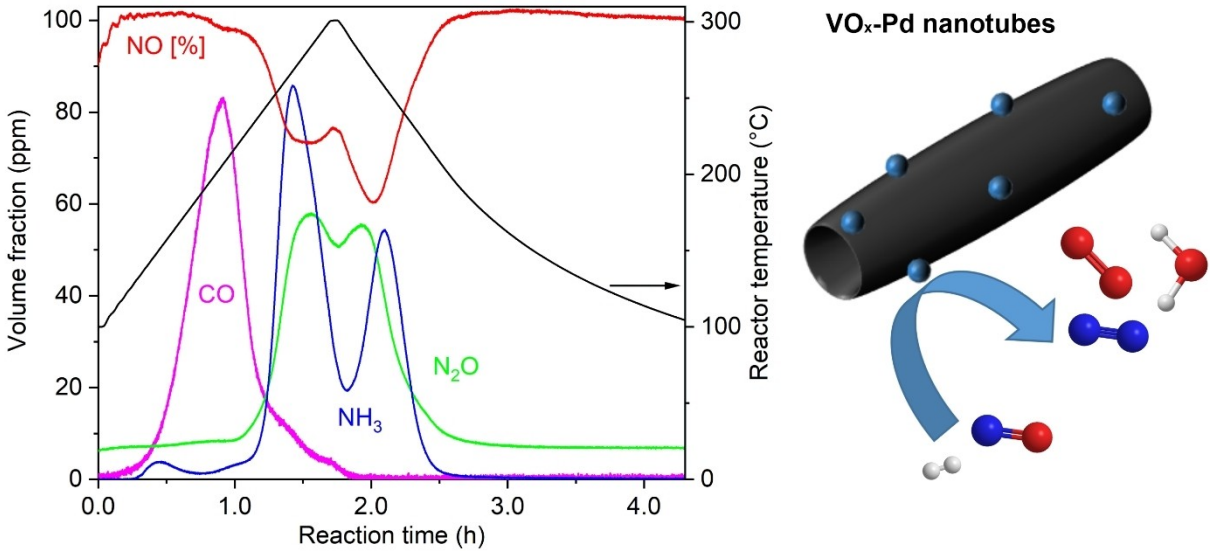


**Figure 6.** $H_2$-SCR process with $VO_x$-Pd nanotubes with concentration profiles of NO (red), $NH_3$ (blue), CO (violet), $N_2O$ (green), as well as the temperature profile (black).


© 2022 The Authors. ChemCatChem published by Wiley-VCH GmbH

18673899, 0, Downloaded from https://chemistry-europe.onlinelibrary.wiley.com/doi/10.1002/cctc.202201354 by Karlsruher Inst F. Technologie, Wiley Online Library on [03/02/2023]. See the Terms and Conditions (https://onlinelibrary.wiley.com/terms-and-conditions) on Wiley Online Library for rules of use; OA articles are governed by the applicable Creative Commons License

minor activity drop, similar to the previously reported behavior of other Pd-based $H_2$-SCR catalysts.[5a,b] Similarly, the side-products $NH_3$ and $N_2O$ pass local maxima during heating, namely a maximum volumetric share of 86 ppm $NH_3$ at 268 °C and of 57 ppm $N_2O$ at 283 °C (Figure 6). In addition, the initial heating ramp gives rise to a pronounced CO signal between 120 and 210 °C (*SI: Figure S6*), which originates from a loss of dodecylamine as a stabilizer that remained adhered on the nanotube surface after preparation. Notably, the maxima of the side products are less intense in the cooling ramp, whereas the NO conversion over the $VO_x$-Pd nanotubes increases to a maximum of approximately 40% at 265 °C (*SI: Figure S7*). This hysteresis behavior most likely relates to the evaporation of residual dodecylamine at temperatures above 180 °C, which was confirmed by both TG analysis and the CO signal during the catalytic tests. Since the stabilizer can potentially block catalytically active surface sites, its removal from the catalyst's surface can be accompanied by an improved catalytic performance. Although CO could also be adsorbed and activated on Pd, in principle, hereby acting as a reductant for $NO_x$,[22] the kinetic data suggest that CO rather acts as an inhibitor of $NO_x$ conversion over the $VO_x$-Pd nanotubes (Figure 6), most likely because CO and NO compete for the same Pd surface sites.[23] According to STEM, moreover, the $VO_x$ nanotubes retain their morphology only up to a temperature of 350 °C (Figure 5f). Hence, major structural or morphological changes of the catalyst, e.g. due to thermal degradation, are not to be expected during a single test run when using such $VO_x$-Pd nanotubes as redox catalyst for NO reduction in the $H_2$-SCR process. However, minor morphological changes of the $VO_x$ nanotubes under the conditions of the reaction-gas mixture in combination with the evaporation of surface-adhered dodecylamine may negatively affect the redox properties of the $VO_x$-Pd nanotube catalyst and/or the noble metal to metal-oxide support interaction on the long run. As these redox properties are key to the activity of $H_2$-SCR catalysts,[6,8,24] the evolution of $VO_x$ nanotube-based $H_2$-SCR catalysts should be subject of future investigations.

Since $H_2$-SCR with $VO_x$-based nanotube catalysts – to the best of our knowledge – is studied for the first time, we have used a 74%$Al_2O_3$/20%$TiO_2$/5%$V_2O_5$/1%Pd catalyst system as a reference system. The catalyst, subject to our present study, were tested with identical conditions as applied by Borchers *et al.*[5b] However, it must be noticed that these authors have used a monolithic sample with a catalytically active washcoat instead of a powder catalyst. In comparison to the maximum NO conversion of 40% observed over the $VO_x$-Pd (2%) nanotubes in our current study (*SI: Figure S7*), the monolithic 74% $Al_2O_3$/20%$TiO_2$/5%$V_2O_5$/1%Pd catalyst exhibited only a slightly higher maximum NO conversion of 48% at about 220 °C. Moreover, the $NH_3$ concentration was negligible between 100 °C and 300 °C, and $N_2O$ represented the most abundant side product with a maximum concentration of 70 ppm. Notably, this comparison underscores the high attractiveness of $VO_x$-Pd nanotubes for $H_2$-SCR. Despite the less complicated catalyst formulation and the lower surface area (74%$Al_2O_3$/20%$TiO_2$/5% $V_2O_5$/1%Pd: 158 $m^2/g$[5b] *versus* $VO_x$ nanotubes with 25 $m^2/g$), the $VO_x$-Pd nanotube catalyst has only a slightly lower NO conversion compared to the monolithic reference catalyst and forms at least slightly lower $N_2O$ emissions. The monolithic reference catalyst, however, outperforms the $VO_x$-Pd nanotubes with respect to $NH_3$ emission. The reference catalyst's lower tendency to form $NH_3$ is likely due to the presence of $TiO_2$, whose addition to the $H_2$-SCR catalyst formulation was recently reported to be a suiTable Strategy to minimize $NH_3$ formation.[9b]

While the aforementioned comparison with a monolithic reference catalyst clearly points to the suitability of the $VO_x$-Pd nanotubes for $H_2$-SCR, further modification is necessary to improve both activity and selectivity. In this regard, ZnO@$VO_x$-Pd nanorods and l-$TiO_2$@$VO_x$-Pd nanotubes with basic ZnO and acidic $TiO_2$ were evaluated as alternative catalyst supports. In contrast to the $VO_x$-Pd nanotubes, both ZnO@$VO_x$-Pd nanorods and l-$TiO_2$@$VO_x$-Pd nanotubes have the additional advantage of the absence of long-chained stabilizers adhered on the catalyst surface such as dodecylamine in the case of the $VO_x$-Pd nanotubes. As a result, the ZnO@$VO_x$-Pd nanorods exhibit a significantly lower NO conversion compared to the $VO_x$-Pd nanotubes, although they efficiently suppress $NH_3$ formation (Figure 7). Since the noble metal loading of both samples is essentially the same, i.e. 2.0 wt-% for $VO_x$-Pd and 2.1 wt-% for ZnO@$VO_x$-Pd, and also the surface areas of the support materials differ only marginally ($VO_x$ nanotubes: 25 $m^2/g$ *versus* ZnO@$VO_x$ nanorods: 27 $m^2/g$), the introduction of ZnO seems to govern the change in catalytic activity. Generally, this finding is in accordance with literature on Pt-based $H_2$-SCR catalysts. Thus, Li *et al.* found that basic supports like MgO inhibit the $H_2$-SCR reaction and favor the formation of oxidized Pt species (i.e., PtO, $PtO_2$), whereas acidic supports promote the $NO_x$ conversion and keep Pt in the metallic state.[24c] Specifically, the oxidation state of Pt is known to affect the $NO_x$ adsorption capacity and the catalytic activity significantly. Similar to MgO as a catalyst support, we ascribe the inferior NO conversion of the ZnO@$VO_x$-Pd nanorods to the basic character of the ZnO support. Compared to the $VO_x$-Pd nanotubes, the $N_2O$ concentration increases substantially for the ZnO@$VO_x$-Pd nanorods (Figure 7), which points to the contribution of the ZnO support to the overall selectivity. In line with previous findings,[24c] moreover, the basic ZnO support also reduces the $N_2$ selectivity (*SI: Figure S8*).

As a most obvious difference to $VO_x$-Pd nanotubes and ZnO@$VO_x$-Pd nanorods, the l-$TiO_2$@$VO_x$-Pd nanotubes considerably improve the $NO_x$ conversion culminating in a maximum NO conversion of 70% at 213 °C during the cooling phase (Figure 8; *SI: Figure S9*). While only minor $NO_2$ concentrations were observed throughout the light-off/light-out cycle, the maximum NO conversion coincides with the maximum of the $N_2O$ concentration (122 ppm). Moreover, the concentrations of $NH_3$ and $NO_2$ are both negligible with l-$TiO_2$@$VO_x$-Pd nanotubes over the entire temperature and time range (Figure 8). The incorporation of $TiO_2$ into the support material may promote the catalytic activity for $H_2$-SCR in twofold manner. First, the surface area of 387 $m^2/g$ that was determined for the l-$TiO_2$@$VO_x$ nanotubes exceeds the surface area of the ZnO@$VO_x$


© 2022 The Authors. ChemCatChem published by Wiley-VCH GmbH

18673899, 0, Downloaded from https://chemistry-europe.onlinelibrary.wiley.com/doi/10.1002/cctc.202201354 by Karlsruher Inst F. Technologie, Wiley Online Library on [03/02/2023]. See the Terms and Conditions (https://onlinelibrary.wiley.com/terms-and-conditions) on Wiley Online Library for rules of use; OA articles are governed by the applicable Creative Commons License

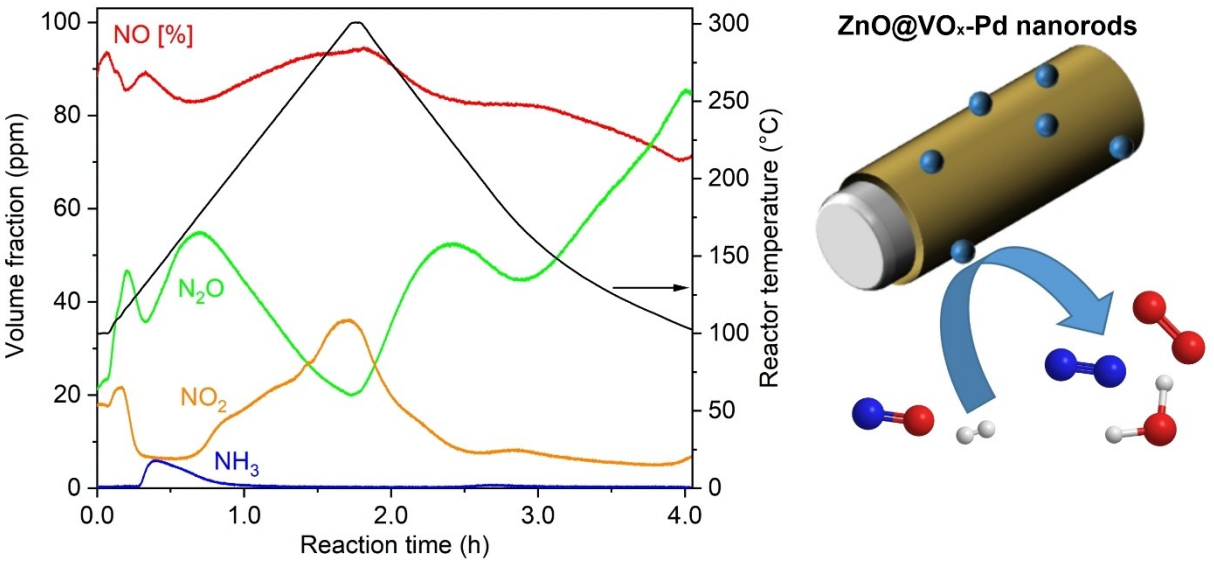


**Figure 7.** $H_2$-SCR process with ZnO@$VO_x$-Pd nanorods with concentration profiles of NO (red), $NH_3$ (blue), $N_2O$ (green), $NO_2$ (orange), as well as the temperature profile (black).

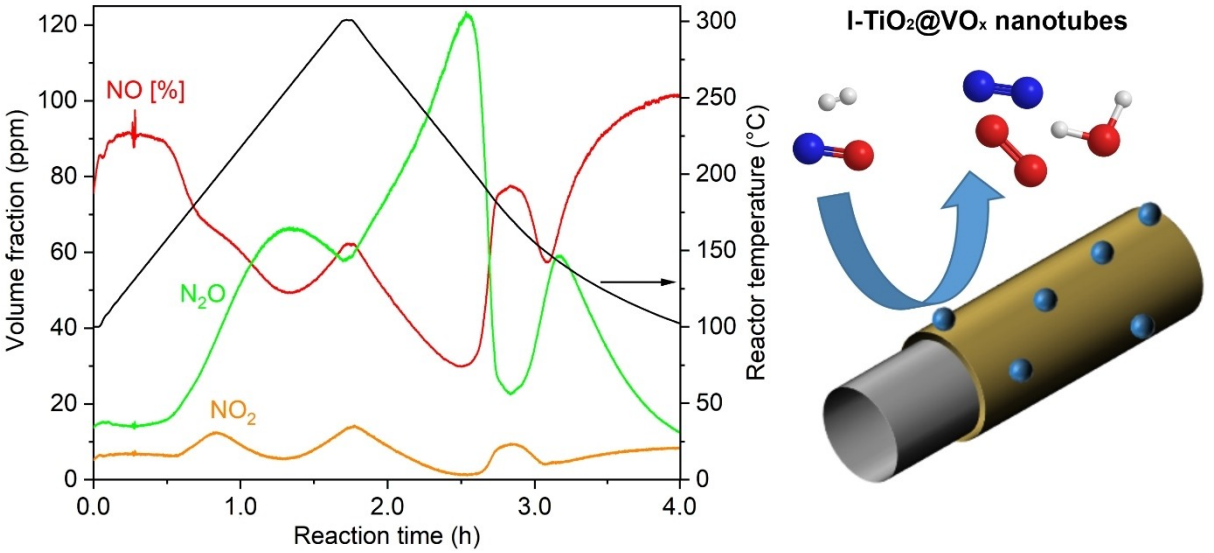


**Figure 8.** $H_2$-SCR process with I-$TiO_2$@$VO_x$-Pd nanotubes with concentration profiles of NO (red), $N_2O$ (green), $NO_2$ (orange), as well as the temperature profile (black).

nanorods (27 $m^2$/g) and $VO_x$ nanotubes (25 $m^2$/g) by far, hereby providing a large surface for the adsorption of reactive species, which ultimately promotes noble metal to metal-oxide support interactions that were found to trigger the $H_2$-SCR reaction.[8] Second, the addition of 10 to 20 wt-% of $TiO_2$ to zeolitic support materials with a high surface area was recently reported as highly beneficial for the activity and product selectivity of Pd-based $H_2$-SCR catalysts, presumably due to an increased reducibility of active Pd sites and an enhanced activation of reactants, which involves both the noble metal as well as the support material.[9b] Hence, we can assume that $TiO_2$ promotes the reduction of $NO_x$ with $H_2$ also for thel-$TiO_2$@$VO_x$ nanotube catalyst.

Taken together, $VO_x$ turned out to be an interesting catalyst material for $H_2$-SCR, which is here evaluated for the first time in the form of nanorods and nanotubes as a morphology since this is considered beneficial in terms of mechanical and chemical stability in combination with high surface area. Similar to previous studies, acidic catalyst supports such as titania result in a higher $NO_x$ conversion rate than basic catalyst supports such as ZnO.[24] From the newly realized $VO_x$-Pd nanotubes, ZnO@$VO_x$-Pd nanorods, and I-$TiO_2$@$VO_x$-Pd nanotubes as $H_2$-SCR catalysts, I-$TiO_2$@$VO_x$-Pd nanotubes outperform


© 2022 The Authors. ChemCatChem published by Wiley-VCH GmbH

18673899, 0, Downloaded from https://chemistry-europe.onlinelibrary.wiley.com/doi/10.1002/cctc.202201354 by Karlsruher Inst F. Technologie, Wiley Online Library on [03/02/2023]. See the Terms and Conditions (https://onlinelibrary.wiley.com/terms-and-conditions) on Wiley Online Library for rules of use; OA articles are governed by the applicable Creative Commons License

the pure $VO_x$-Pd nanotubes due to the absence of long-chained, high-molecular weight stabilizers remaining adhered on the catalyst surface, the high surface area, and the beneficial presence of acidic $TiO_2$. The l-$TiO_2$@$VO_x$-Pd nanotubes, finally, show the best performance with promising activity (up to 70%) and selectivity (up to 80% $N_2$), which can be further improved by fine-tuning of structure and composition.

## Conclusion

Vanadium oxide ($VO_x$-Pd) nanorod-/nanotube-based catalysts were evaluated for selective catalytic reduction of $NO_x$ with hydrogen ($H_2$-SCR) for the first time and show promising catalytic performance. In detail, $VO_x$-Pd nanotubes (length: 700±300 nm, diameter: 100±25 nm, inner tube diameter: 10 nm), ZnO@$VO_x$-Pd nanorods (length: 700±300 nm, diameter: 40±10 nm), and l-$TiO_2$@$VO_x$-Pd nanotubes (length: 300±50 nm, diameter: 15±5 nm, inner tube diameter: 7±1 nm) were prepared and decorated with Pd nanoparticles (2.0–2.5 wt-% Pd, diameter: 14±5 nm). Due to the similar redox potential of the $VO_2^+/VO^{2+}$ and $Pd^{2+}$/Pd redox couples (both with 1.0 V), unfortunately, the reduction of $Pd^{2+}$ cannot be accelerated, which limits the size of the Pd nanoparticles. All catalysts show interesting catalytic performance in regard of the catalytic reduction of NO with $H_2$. Thus, an activity/selectivity (to $N_2$) of 40%/63% for $VO_x$-Pd nanotubes, 30%/50% for ZnO@$VO_x$-Pd nanorods, and 70%/80% for l-$TiO_2$@$VO_x$-Pd nanotubes were determined. Furthermore, thermal stability of the respective nanostructure up to 350 °C ($VO_x$), and 500 °C (ZnO@$VO_x$, l-$TiO_2$@$VO_x$) was observed.

Taken together, $VO_x$-based nanorods/nanotubes are first evaluated for $H_2$-SCR. Hereof, l-$TiO_2$@$VO_x$-Pd nanotubes show the most promising performance with superior activity (up to 70% NO conversion) and selectivity (up to 80% $N_2$ selectivity) as well as a good thermal stability (>500 °C). Based on the first evaluation of these $VO_x$-based catalysts, further optimization of, e.g., $VO_x$ load, Pd load, size of Pd nanoparticles, can result in an even further improved activity and selectivity.

## Experimental Section

*General.* Vanadium(V) oxide (98.7%, ABCR), titanium (98.7%, ABCR), NaOH (≥97.0%, VWR), KOH (≥97.0%, VWR), $H_2O_2$ (medical pure, 30%, Sigma-Aldrich), $Zn(OAc)_2 \cdot 2\ H_2O$ (≥99%, Sigma-Aldrich), $VO(SO_4) \cdot H_2O$ (99.9%, Alfa Aesar), $Pd(OAc)_2$ (47.5% Pd, Acros Organics), dodecylamine (98%, Sigma-Aldrich), $NH_3$ solution (25%, Seulberger), $HNO_3$ (technical grade, 65%, AppliChem), acetone (technical, Seulberger), hexane (technical grade, Seulberger), methanol (technical grade, Seulberger) and ethanol (technical grade, Seulberger) were used as purchased.

*$VO_x$-Pd (2 wt-%) nanotubes.* The synthesis was conducted according to a procedure reported by Spahr *et al.*[13] Accordingly, 1.37 g of $V_2O_5$ and 1.39 g of dodecylamine were dispersed in 5 mL of EtOH and stirred for 1 h. Subsequently, 15 mL of $H_2O$ were added and the yellow mixture stirred for another 6 h. Thereafter, the mixture was placed into a teflon-lined autoclave and heated to 180 °C for 7 days. After natural cooling, the black suspension was washed thrice with ethanol and hexane, respectively. The as-prepared dark green solid was dried at room temperature.

To coat the $VO_x$ nanotubes with Pd nanoparticles, palladium acetate was dissolved in 15 mL of acetone. The yellow solution was then added to the aforementioned $VO_x$ nanotubes by drop-casting. The resulting green powder was dried in vacuum and directly purged with $H_2:N_2$ (10:90).

*ZnO nanorods.* The synthesis of the ZnO nanorods was conducted following a recipe by Tripathi *et al.*[17] Thus, 14.75 g of $Zn(OAc)_2 \cdot 2\ H_2O$ were dissolved in 62.5 mL of methanol and heated for 30 min to 65 °C. To this suspension, 7.4 g of KOH in 32.5 mL of methanol were added and heated and concentrated to half of the original volume. Afterwards, the colorless suspension was transferred into a stainless steel autoclave with a teflon inlay and heated to 120 °C for 6 hours. After centrifugation and washing – twice with ethanol and twice with deionized water – the colorless precipitate was dried at room temperature.

*ZnO@$VO_x$-Pd (2 wt-%) nanorods.* To deposit a thin layer of $VO_x$, 0.4 g of the ZnO nanorods were dispersed in 150 mL of deionized water and ultrasonicated for 5 min. To this suspension, a slight blue solution of 0.1 g of $VOSO_4 \cdot H_2O$ in 100 mL of deionized water was added with a syringe pump at a rate of 1 mL/min. Finally, the grey suspension was centrifuged, washed thrice with acetone, and dried at room temperature.

Finally, the ZnO@$VO_x$ nanorods were coated with Pd nanoparticles. To this concern, palladium acetate was dissolved in 15 mL of acetone. The yellow solution was then added to the aforementioned ZnO@$VO_x$ nanorods by drop-casting. Finally, the resulting grey powder was dried in vacuum and directly purged with $H_2:N_2$ (10:90).

*Layered-titania nanotubes.* L-$TiO_2$ nanotubes were prepared according to a procedure of Kasuga *et al.*[25] 170 mg of Ti powder were dispersed in 52.5 mL of 10 M NaOH with 37.5 mL of 30% $H_2O_2$ and heated in a teflon-lined autoclave to 120 °C for 24 h. After natural cooling, the colorless suspension was washed thrice with deionized water and resuspended in 50 mL of 0.175 M $HNO_3$. The suspension was mixed on an orbital shaker for 12 h. The acidic treatment with $HNO_3$ was repeated once. After washing thrice with deionized water, the sample was dried at 70 °C.

*L-$TiO_2$@$VO_x$-Pd (2 wt-%) nanotubes.* For deposition of $VO_x$, 0.5 g of the l-$TiO_2$ nanotubes were dispersed in 250 mL of deionized water and ultrasonicated for 5 min. To this suspension, a light blue solution of 0.175 g of $VO(SO_4) \cdot H_2O$ in 125 mL of deionized water was added with a syringe pump at a rate of 1 mL/min. After the addition, the yellow suspension was treated with 15 mL of 2.5% $NH_3$ solution to adjust pH 6. After centrifugation, washing with acetone and deionized water, and drying at room temperature a yellow powder was obtained.

The l-$TiO_2$@$VO_x$ nanotubes were coated with Pd nanoparticles as discussed above. Thus, palladium acetate was dissolved in 15 mL of acetone. This yellow solution was added to the l-$TiO_2$@$VO_x$ nanotubes by drop-casting. The resulting yellow powder was dried in vacuum and directly purged with $H_2:N_2$ (10:90).

*Field emission scanning electron microscopy* (FESEM, Zeiss Supra 40VP) was used to determine the morphology of the as-prepared nanorods and nanotubes and their modification in the STEM mode. Samples were prepared by casting a drop of an aqueous suspension onto a 300 mesh copper grid with carbon support film.

*Transmission electron microscopy* (TEM equipped with energy dispersive X-ray spectrometer, EDXS) was conducted to investigate the size, the morphology and the spatial distribution of the Pd


© 2022 The Authors. ChemCatChem published by Wiley-VCH GmbH

18673899, 0, Downloaded from https://chemistry-europe.onlinelibrary.wiley.com/doi/10.1002/cctc.202201354 by Karlsruher Inst F. Technologie, Wiley Online Library on [03/02/2023]. See the Terms and Conditions (https://onlinelibrary.wiley.com/terms-and-conditions) on Wiley Online Library for rules of use; OA articles are governed by the applicable Creative Commons License

nanoparticles on the metal oxide nanorods and nanotubes at 200 kV. To this concern, a FEI Tecnai Osiris microscope (FEI, USA) was used. Samples were prepared by casting one drop of aqueous suspension onto a 300 mesh copper grid with carbon support film.

*X-ray powder diffraction (XRD).* Crystallinity and chemical composition of the modified and non-modified nanorods and nanotubes were examined by XRD (Stoe STADI-MP diffractometer, equipped with Ge-monochromator and Cu-$K_{\alpha 1}$ radiation, 40 kV, 40 mA). About 10 mg of the respective sample was deposited onto acetate foil and fixed with scotch tape.

*Volumetric nitrogen sorption measurements* (BEL BELSORP-max) were carried out at 77 K with nitrogen as analyte. According to the BET formalism (BET: Brunauer-Emmett-Teller), the specific surface area was deduced. Prior to the analysis, the samples were dried at 120 °C in vacuum.

*Thermogravimetric analysis* (TGA) was used to study the thermal stability of the catalysts with a STA409C device (Netzsch, Germany). Measurements were conducted in $O_2/N_2$ (20:80) atmosphere to ensure a complete combustion of the organic content. The dried catalyst materials (15–20 mg, corundum crucibles) were heated from 30 °C to 1000 °C with a heating rate of 1 K/min.

*Selective catalytic reduction of $NO_x$ with $H_2$ ($H_2$-SCR)* was performed in a powder catalyst testing bench by exposing a fixed bed to a continuous gas flow during continuous heating from 100 °C to 300 °C with 3 K/min and subsequent cooling. The fixed bed consisted of 150 mg of the nanorod/nanotube powder sample mixed with 850 mg of $SiO_2$ (grain size 125–250 µm) and was mounted between two quartz wool plugs in a quartz glass tubular flow reactor that was placed in a furnace. Two thermocouples (type N; TC Mess- und Regeltechnik GmbH) up- and downstream the catalyst bed ensured precise temperature control and mass flow controllers (MFCs; Bronkhorst Deutschland Nord GmbH) allowed dosing a well-defined gas mixture of 0.1 % NO, 0.5 % $H_2$ and 10 % $O_2$ in $N_2$ at a gas hourly space velocity (GHSV) of 80,000 $h^{-1}$. A Fourier-transform infrared spectrometer (FT-IR, MG2030; MKS Instruments, USA) provided precise end-of-pipe gas composition data with an interval of one second. The entire setup was controlled by an in-house developed LabView software, which simultaneously monitored all relevant data (set points and real values for gas composition and temperature).

## Acknowledgements

*The authors acknowledge the Deutsche Forschungsgemeinschaft (DFG) for funding within the Collaborative Research Center 1441* „Tracking the Active Site in Heterogeneous Catalysis for Emission Control (TrackAct)“ *(Project-ID 426888090). Furthermore, they are grateful to Jakob Hauns (IPC, KIT) for performing XPS measurements and to Michael Borchers (ITCP, KIT) for his support during the catalytic activity tests. Finally, L.W. acknowledges the Studienstiftung des deutschen Volkes for scholarship. Open Access funding enabled and organized by Projekt DEAL.*

## Conflict of Interest

The authors declare no conflict of interest.

## Data Availability Statement

The data that support the findings of this study are available from the corresponding author upon reasonable request.

**Keywords:** $H_2$-SCR · nanorods/-tubes · titania · vanadium oxide · zinc oxide

[1] a) E. Tronconi, I. Nova, C. Ciardelli, D. Chatterjee, M. Weibel, *J. Catal.* **2007**, *245*, 1–10; b) J. Due-Hansen, S. B. Rasmussen, E. Mikolajska, M. A. Bañares, P. Avila, R. Fehrmann, *Appl. Catal. B* **2011**, *107*, 340–346; c) V. V. Kaichev, Y. A. Chesalov, A. A. Saraev, A. M. Tsapina, *J. Phys. Chem. C* **2019**, *123*, 19668–19680; d) P. Nagaraju, Y. Vijayakumar, M. V. R. Reddy, U. P. Deshpande, *RSC Adv.* **2019**, *9*, 16515–16524; e) T. Yan, Q. Liu, S. Wang, G. Xu, M. Wu, J. Chen, J. Li, *ACS Catal.* **2020**, *10*, 2747–2753.
[2] C. W. Zou, Y. F. Rao, A. Alyamani, W. Chu, M. J. Chen, D. A. Patterson, E. A. C. Emanuelsson, W. Gao, *Langmuir* **2010**, *26*, 11615–11620.
[3] Y.-M. Chai, X.-Y. Zhang, J.-H. Lin, J.-F. Qin, Z.-Z. Liu, J.-Y. Xie, B.-Y. Guo, Z. Yang, B. Dong, *Int. J. Hydrogen Energy* **2019**, *44*, 10156–10162.
[4] a) G. Busca, L. Lietti, G. Ramis, F. Berti, *Appl. Catal. B* **1998**, *18*, 1–36; b) J.-K. Lai, I. E. Wachs, *ACS Catal.* **2018**, *8*, 6537–6551.
[5] a) G. Qi, R. Yang, F. Rinaldi, *J. Catal.* **2006**, *237*, 381–392; b) M. Borchers, K. Keller, P. Lott, O. Deutschmann, *Ind. Eng. Chem. Res.* **2021**, *60*, 6613–6626; c) P. Lott, U. Wagner, T. Koch, O. Deutschmann, *Chem. Ing. Tech.* **2022**, *94*, 217–229.
[6] N. Macleod, R. M. Lambert, *Catal. Lett.* **2003**, *90*, 111–115.
[7] a) A. Russell, W. S. Epling, *Catal. Rev.* **2011**, *53*, 337–423; b) P. Lott, O. Deutschmann, *Emiss. Control Sci. Technol.* **2021**, *7*, 1–6.
[8] L. Wang, C. Yin, R. T. Yang, *Appl. Catal. A* **2016**, *514*, 35–42.
[9] a) Z. Hu, R. T. Yang, *Ind. Eng. Chem. Res.* **2019**, *58*, 10140–10153; b) M. Borchers, P. Lott, O. Deutschmann, *Top. Catal.* **2022**, DOI: 10.1007/s11244-022-01723-1; c) E. Esser, S. Kureti, L. Heckemüller, A. Todt, P. Eilts, T. Morawietz, A. Friedrich, W. Waiblinger, S. Hosseiny, F. Bunar, *SAE Int. J. Adv. & Curr. Prac. in Mobility* **2022**, *4*, 1828–1845.
[10] a) S. P. Vattikuti, P. A. K. Reddy, P. C. NagaJyothi, J. Shim, C. Byon, *J. Alloys Compd.* **2018**, *740*, 574–586; b) R. Camposeco, S. Castillo, M. Hinojosa-Reyes, V. Rodriguez-Gonzalez, N. Nava, I. Mejía-Centeno, *Chem. Select* **2019**, *4*, 1023–1030.
[11] K.-F. Zhang, D.-J. Guo, X. Liu, J. Li, H.-L. Li, Z.-X. Su, *J. Power Sources* **2006**, *162*, 1077–1081.
[12] a) I. Song, H. Lee, D. H. Kim, *ACS Appl. Mater. Interfaces* **2018**, *10*, 42249–42257; b) I. Song, S. Youn, H. Lee, S. G. Lee, S. J. Cho, D. H. Kim, *Appl. Catal. B* **2017**, *210*, 421–431; c) H. Wang, P. Wang, X. Chen, Z. Wu, *J. Hazard. Mater.* **2017**, *324*, 507–515.
[13] M. E. Spahr, P. Bitterli, R. Nesper, M. Müller, F. Krumeich, H. U. Nissen, *Angew. Chem. Int. Ed.* **1998**, *37*, 1263–1265; *Angew. Chem.* **1998**, *110*, 1339–1342.
[14] a) F. Krumeich, H.-J. Muhr, M. Niederberger, F. Bieri, B. Schnyder, R. Nesper, *J. Am. Chem. Soc.* **1999**, *121*, 8324–8331; b) I. Derkaoui, M. Khenfouch, I. Boukhoubza, M. Achehboune, R. Hatel, B. M. Mothudi, I. Zorkani, A. Jorio, M. Maaza, *Appl. Phys. A* **2021**, *127*, 934.
[15] a) H.-J. Muhr, F. Krumeich, U. P. Schönholzer, F. Bieri, M. Niederberger, L. J. Gauckler, R. Nesper, *Adv. Mater.* **2000**, *12*, 231–234; b) M. Niederberger, H.-J. Muhr, F. Krumeich, F. Bieri, D. Günther, R. Nesper, *Chem. Mater.* **2000**, *12*, 1995–2000.
[16] A. F. Holleman, N. Wiberg, *Anorganische Chemie*, de Gruyter, 103rd ed, Berlin **2016**.
[17] S. Tripathi, R. Bose, A. Roy, S. Nair, N. Ravishankar, *ACS Appl. Mater. Interfaces* **2015**, *7*, 26430–26436.
[18] a) H. Chang, M.-H. Tsai, *Rev. Adv. Mater. Sci.* **2008**, *18*, 734–743; b) K.-M. Kim, T.-H. Kim, H.-M. Kim, H.-J. Kim, G.-H. Gwak, S.-M. Paek, J.-M. Oh, *Toxicol. Environ. Health Sci.* **2012**, *4*, 121–131; c) R. Marsalek, *APCBEE Proced.* **2014**, *9*, 13–17; d) N. Senthilkumar, E. Vivek, M. Shankar, M. Meena, M. Vimalan, I. V. Potheher, *J. Mater. Sci.* **2018**, *29*, 2927–2938.
[19] L. Warmuth, G. Nails, M. Casapu, S. Wang, S. Behrens, J.-D. Grunwaldt, C. Feldmann, *Catalysts* **2021**, *11*, 949.
[20] a) A.-L. Papa, J. Boudon, V. Bellat, A. Loiseau, H. Bisht, F. Sallem, R. Chassagnon, V. Bérard, N. Millot, *Dalton Trans.* **2015**, *44*, 739–746; b) A.-L. Papa, L. Maurizi, D. Vandroux, P. Walker, N. Millot, *J. Phys. Chem. C* **2011**, *115*, 19012–19017.


© 2022 The Authors. ChemCatChem published by Wiley-VCH GmbH

18673899, 0, Downloaded from https://chemistry-europe.onlinelibrary.wiley.com/doi/10.1002/cctc.202201354 by Karlsruher Inst F. Technologie, Wiley Online Library on [03/02/2023]. See the Terms and Conditions (https://onlinelibrary.wiley.com/terms-and-conditions) on Wiley Online Library for rules of use; OA articles are governed by the applicable Creative Commons License

[21] B. Cornils, *Hüttig temperature. In: B. Cornils, W. A. Herrmann, J.-H. Xu, H. Zanthoff (Eds): Catalysis from A to Z: A Concise Encyclopedia*, Wiley-VCH, Weinheim **2019**.
[22] M. Konsolakis, M. Vrontaki, G. Avgouropoulos, T. Ioannides, I. V. Yentekakis, *Appl. Catal. B* **2006**, *68*, 59–67.
[23] J. M. Lorenzi, S. Matera, K. Reuter, *ACS Catal.* **2016**, *6*, 5191–5197.
[24] a) A. Ueda, T. Nakao, M. Azuma, T. Kobayashi, *Catal. Today* **1998**, *45*, 135–138; b) M. Saito, M. Itoh, J. Iwamoto, K. Machida, *Chem. Lett.* **2008**, *37*, 1210–1211; c) X. Li, X. Zhang, Y. Xu, Y. Liu, X. Wang, *Chin. J. Catal.* **2015**, *36*, 197–203.
[25] a) T. Kasuga, M. Hiramatsu, A. Hoson, T. Sekino, K. Niihara, *Langmuir* **1998**, *14*, 3160–3163; b) T. Kasuga, M. Hiramatsu, A. Hoson, T. Sekino, K. Niihara, *Adv. Mater.* **1999**, *11*, 1307–1311.

Manuscript received: November 3, 2022
Revised manuscript received: December 19, 2022
Accepted manuscript online: December 20, 2022
Version of record online: [redacted], [redacted]


© 2022 The Authors. ChemCatChem published by Wiley-VCH GmbH

18673899, 0, Downloaded from https://chemistry-europe.onlinelibrary.wiley.com/doi/10.1002/cctc.202201354 by Karlsruher Inst. F. Technologie, Wiley Online Library on [03/02/2023]. See the Terms and Conditions (https://onlinelibrary.wiley.com/terms-and-conditions) on Wiley Online Library for rules of use; OA articles are governed by the applicable Creative Commons License


*Dr. L. Warmuth, Dr. P. Lott, Prof. O. Deutschmann*, Prof. C. Feldmann**



**Nanostructured Catalysts for Selective Reduction of NO**: Vanadium oxide ($VO_x$) nanotubes, $VO_x$-coated ZnO nanorods, and $VO_x$-coated, layered-titania nanotubes are decorated with Pd nanoparticles and evaluated for selective catalytic reduction with hydrogen ($H_2$-SCR) for the first time. The materials exhibit a promising catalytic performance, making them attractive for $H_2$-SCR applications.

18673899, 0, Downloaded from https://chemistry-europe.onlinelibrary.wiley.com/doi/10.1002/cctc.202201354 by Karlsruher Inst. F. Technologie, Wiley Online Library on [03/02/2023]. See the Terms and Conditions (https://onlinelibrary.wiley.com/terms-and-conditions) on Wiley Online Library for rules of use; OA articles are governed by the applicable Creative Commons License